Numerical Simulation of Shock Wave – Turbulent Boundary-Layer Interaction

J. S. Shang,* W. L. Hankey Jr.,†
Air Force Flight Dynamics Laboratory, Wright-Patterson AFB, Ohio

and

C. Herbert Law‡
Air Force Aero Propulsion Laboratory, Wright-Patterson AFB, Ohio

Numerical solutions of the Navier-Stokes equations are presented for the interactions of a shock wave and a turbulent boundary layer. The turbulent closure is provided by a relaxation eddy viscosity model that approximates the response of turbulence to a severe pressure gradient. The relaxation eddy viscosity model was successfully applied for a series of compression ramp configurations in a previous investigation by the authors. In the present analysis, further verification of the eddy viscosity model is attempted by investigating shock impingement on a turbulent boundary layer. Computations were performed for shock generators varying from 7.93° to 12.17°, at a freestream Mach number of 2.96 and a Reynolds number of 1.2×10^7. Numerical results obtained with MacCormack's scheme were compared with experimental measurements of the surface pressure distribution and the location of the separation and reattachment points. The density distribution throughout the entire interacting flowfield was also compared with experimental results obtained from holographic interferograms. In general, all essential features of the experimental observation were duplicated by the numerical computation.

Nomenclature

C_f = skin friction coefficient
D = Van Driest damping factor, Eq. (14)
e = specific energy
F,G = vector fluxes in mean flow equations
h = maximum vertical dimension of the computational domain
k = von Karman constant (0.4)
L = length of the leading plate, 1 ft
p = static pressure
P_r = molecular Prandtl number
P_{r_t} = turbulent Prandtl number
t = time
T = temperature
u,v = velocity components in Cartesian coordinates
$u_{\max}$ = maximum velocity in the shock layer
U = vector of conserved properties in mean flow equations
x,y = Cartesian coordinates
δ = boundary-layer thickness
δ_{sg} = deflection angle of the shock generator referenced to the unperturbed freestream
ϵ = eddy viscosity coefficient
λ = relaxation eddy viscosity length scale, Eq. (21)
μ = molecular viscosity coefficient
τ_{ij} = components of the stress matrix

Subscripts

e = denotes properties evaluated at the external stream
0 = denotes properties evaluated at the location immediately upstream of the interaction region
w = denotes properties evaluated at the wall
∞ = denotes properties evaluated at the unperturbed freestream

Received Dec. 22, 1975; presented as Paper 76-95 at the AIAA 14th Aerospace Sciences Meeting, Washington, D. C., Jan. 26-28, 1976; revision received June 17, 1976.

Index categories: Jets, Wakes, and Viscid-Inviscid Flow Interactions; Supersonic and Hypersonic Flow.

*Aerospace Engineer, Flight Mechanics Division. Member AIAA.
†Senior Scientist, Flight Mechanics Division. Member AIAA.
‡Aerospace Engineer, Turbine Engine Division. Member AIAA.

I. Introduction

In recent years, significant progress has been made in the numerical analysis of supersonic flows with strong viscous-inviscid interaction. Two geometries that have received considerable attention are the flat plate-ramp configuration and shock impingement on a plate. The sufficiently large pressure gradient generated either by the ramp geometry or the incident shock wave induces boundary-layer separation. The complex flowfield is characterized by the strong interaction of the viscous dominated region adjacent to the wall with the inviscid freestream. Qualitative similarity has been observed for laminar, transitional, and turbulent flows.

All available techniques in fluid mechanics research have been used to describe laminar viscous-inviscid interactions. Numerical solutions either by means of interacting boundary-layer equations[1-3] or Navier-Stokes equations[4-7] have produced convincing results and reached favorable agreement with experimental measurements. Analytical results also have been obtained. In this regard, the mathematical structure of the separation region has been given by Stewartson and Williams,[8] whereas numerical investigations based upon the asymptotic theory have been successfully carried out by Burggraf et al.[9,10]

Unfortunately, for turbulent flow we have not as yet been able to solve the interacting flowfield as conslusively. The major difficulty can be easily identified as the lack of an accurate turbulence model for the viscous-inviscid interacting flowfield. In spite of the inherent shortcoming, Wilcox[11] first demonstrated the feasibility of numerically solving the turbulent interacting problem. In his work, an explicit time-marching first-order finite difference scheme (AFTON 2 pt code) incorporating Saffman's turbulence model[12] was used. Baldwin and MacCormack[13] also numerically solved a shock boundary-layer interaction problem in the hypersonic regime using two different eddy viscosity models.[12,14] In their work, a multi-layered grid spacing was used to achieve suitable

numerical resolution near the wall. Horstman et al.[15] performed a combined experimental and numerical investigation of a shock-wave-induced flow separation over an axisymmetric configuration. They devised a modification of the diffusion eddy viscosity model by use of their experimental measurements. The comparison between data and calculations by the modified eddy viscosity model reflects reasonable agreement. Shang and Hankey[16,17] also adopted MacCormack's numerical scheme to solve the viscous-inviscid interaction problem in a compression corner with a relaxation eddy viscosity model. The numerical results in comparison with Law's data[18] indicated an improvement over Wilcox's calculation[11] of the compression ramp (mainly in the prediction of the upstream pressure propagation) and a substantial improvement over the result by the conventional equilibrium eddy viscosity model.[14,16,17]

The relaxation eddy viscosity model is first of all an engineering approximation. In concept, it approximates the experimental observation that in a highly decelerated or accelerated turbulent flow, the Reynolds shear stress remains nearly frozen at its initial value while being convected along streamlines[19,20] and then exponentially approaches a new equilibrium state.[20] In practical implementation, the relaxation eddy viscosity model parallels Bradshaw's[21] extra-rate-of-strain correction and also is similar to Rose and Johnson's suggestion for a mixing length correction.[22] An outstanding feature of this turbulence model is its simplicity, in that only one additional parameter is required. (λ, a time-like length scale describing the exponential decay of the eddy viscosity distribution), and as a result pays no penalty in computing time. In numerical computation, an initial streamwise location for which the relaxation phenomenon is initiated also requires specification. The relaxation eddy viscosity model has been successfully demonstrated for a series of compression ramp configurations. Further substantiation of this concept is still needed, particularly if an exact description of the turbulent structure is not feasible for some time to come.

The objectives of the present effort are to demonstrate the sensitivity of the relaxation length scale in the turbulence model and to develop an engineering method capable of predicting the turbulent viscous-inviscid interactions, including flow separation. Since there are few numerical results[11,13,15] and essentially no analytical work to compare and verify accuracy, the substantiation must be obtained from comparison with experimental measurements. However, one should realize that the resolution of suspected three-dimensional influences has not as yet been completely delineated for all the existing experiments.[23,24] Therefore, the specific comparison of experimental data and numerical calculations must concentrate on the essential features of the interaction problem.

II. Governing Equations

The governing equations of the present analysis are the unsteady compressible Navier-Stokes equations in terms of mass-averaged variables.[11,13,15] The turbulent closure is provided by the relaxation eddy viscosity model and the turbulent Prandtl number

$$\frac{\partial U}{\partial t}+\frac{\partial F}{\partial x}+\frac{\partial G}{\partial y}=0 \tag{1}$$

The vector components are

$$U=\begin{Bmatrix}\rho\\ \rho u\\ \rho v\\ \rho e\end{Bmatrix} \tag{2}$$

$$F=\begin{Bmatrix}\rho u\\ \rho u^2-\sigma_{xx}\\ \rho uv-\tau_{xy}\\ (\rho e-\sigma_{xx})u-\tau_{xy}\cdot v-\dot{q}_x\end{Bmatrix} \tag{3}$$

$$G=\begin{Bmatrix}\rho v\\ \rho uv-\tau_{xy}\\ \rho v^2-\sigma_{yy}\\ (\rho e-\sigma_{yy})v-\tau_{xy}\cdot u-\dot{q}_y\end{Bmatrix} \tag{4}$$

where the apparent stress components and the mean specific total energy e, are given in Ref. 16. Auxiliary relationships included in the system of equations are the equation of state for a perfect gas and Sutherland's viscosity equation. Prandtl numbers utilized are the molecular $P_r=0.72$ and the turbulent $P_{r_t}=0.90$.

The associated boundary conditions are prescribed as follows: The initial condition and upstream boundary condition are prescribed at the freestream value for all the dependent variables

$$U(0,x,y)=U_\infty \tag{5a}$$

$$U(t,x_i,y)=U_\infty \tag{5b}$$

At the downstream boundary, the component of the gradient of the dependent variables in the streamwise direction is set to zero

$$\frac{\partial U}{\partial x}=0 \tag{6}$$

The outer boundary conditions for the present analysis consists of two segments,[16] upstream and downstream of the incident shock. The boundary condition on the former is satisfied by permitting the flow to approach its unperturbed freestream value

$$U(t,x,h)=U_\infty \tag{7}$$

The boundary condition on the segment downstream of the incident shock is fulfilled by the Rankine-Hugoniot relations

$$U(t,x,h)=U(M_\infty,\delta\text{sg}) \tag{8}$$

The anticipated reflected shock is permitted to pass through the downstream segment of the computational domain. Therefore, no additional prescribed boundary condition is required.

The boundary conditions on the solid contour are given as the nonslip condition for velocity

$$u(t,x,0)=0 \tag{9}$$

$$v(t,x,0)=0 \tag{10}$$

and the adiabatic wall

$$\left.\frac{\partial T}{\partial y}\right|_{y=0}=0 \tag{11}$$

The pressure at the wall is obtained by satisfying the compatible condition.

$$\left.\frac{\partial p}{\partial y}\right|_{y=0}=\left[\frac{\partial}{\partial x}\left(\mu\frac{\partial u}{\partial y}\right)+\frac{\partial}{\partial y}\left(\frac{4}{3}\mu\frac{\partial v}{\partial y}\right)-\frac{\partial}{\partial y}\left(\frac{2}{3}\mu\frac{\partial u}{\partial x}\right)\right]_{y=0} \tag{12}$$

III. Eddy Viscosity Model

The relaxation eddy viscosity model consists of a system of three equations. The local equilibrium eddy viscosity coefficient is described by the Cebeci-Smith's model.[14]

In the inner region

$$\epsilon_{eq(i)} = \rho k^2 y^2 D^2 \left| \frac{\partial u}{\partial y} \right| \tag{13}$$

where k is the von Karman constant (0.4) and D is the Van Driest damping factor:

$$D = 1 - \exp\left(-y \frac{\sqrt{|\tau_w|}}{\rho_w} / 26\nu_w\right) \tag{14}$$

The outer region, Clauser's defect law gives

$$\epsilon_{eq(o)} = 0.0168 \rho u_{max} \delta_i^* \tag{15}$$

δ_i^* is the kinematic displacement thickness (also the basic scaling for the outer layer).

$$\delta_i^* = \int_0^h \left(1 - \frac{u}{u_{max}}\right) dy \tag{16}$$

One notes that the reference velocity is taken as u_{max} in the calculation of the kinematic displacement thickness (δ_i^*) to prevent a possible numerical anomaly in the transient phase of the computations. More importantly, one must also appreciate that the outer edge of an interacting boundary layer cannot be readily defined, and for this reason the intermittency correction of the wake region is also omitted.

In the relaxation eddy viscosity model, the flow "history" effects or, more precisely, the Reynolds stress relaxation phenomenon is described by a simple algebraic equation for the eddy viscosity coefficient

$$\epsilon = \epsilon_0 + (\epsilon_{eq.} - \epsilon_0)\ \left(1 - \exp - \left(\frac{\Delta x}{\lambda}\right)\right) \tag{17}$$

where ϵ denotes the relaxing eddy viscosity coefficient. The local equilibrium value of the eddy viscosity ϵ_{eq} is generated by Eqs. (13) and (15). The distance between the initial station and the calculated station is indicated as Δx, and the parameter λ is the relaxation length scale. The value for ϵ_0 is defined as the eddy viscosity at an upstream location, for which the relaxation phenomena is initiated. This reference station for defining ϵ_0 was selected at $x/L = 0.9027$ for all the computations presented, which corresponds to about seven boundary-layer thicknesses upstream of the intersection of the shock wave and the wall.

The relaxation parameter λ, which is a measure of the memory of stress-containing eddies, is the only free parameter to describe numerically the relaxation phenomenon. Bradshaw[21] has shown that this parameter is the ratio of the turbulent energy to the rate of production of the turbulent energy. He also estimated a factor of five difference in λ between a boundary layer and a jet or free mixing layer. In the present analysis, the sensitivity of the relaxation length scale is demonstrated by utilizing two values of λ; namely, $\lambda = 10\delta_0$ and $\lambda = 20\delta_0$. The former has been used exclusively in Refs. 16 and 17.

Equation (21) is a particular solution of a rate equation suggested by Bradshaw[21] in his study on the effects of streamline curvature in turbulent flow. Equation (21) is also similar to the relaxation equation for the mixing length suggested by Rose and Johnson.[22] According to Bradshaw,[21] the relaxation length parameter λ is a function of y to take into account different turbulent scalings in the inner and outer regions. He postulated that the fine eddy structure near the wall quickly achieves an equilibrium state, whereas the outer region requires a longer period to readjust. However, in carrying out this concept for turbulent interactions in a previous investigation,[17] little numerical difference was observed.

IV. Numerical Procedure

MacCormack's[4,6] alternating-direction-explicit numerical scheme is adopted in the present analysis. Two numerical damping terms are included specially designed to eliminate nonlinear instabilities. One of these, recently implemented by MacCormack and Baldwin, is applied to the convective terms,[6] whereas, for flowfields containing severe pressure gradients such as in this boundary-layer-shock wave interaction, a fourth-order smoothing term[4,6,7,13] is necessary. The detailed description of the numerical smoothing procedure can be found in Ref. 4.

A major difficulty encountered in the numerical analysis is the determination of the resolution required for engineering accuracy. The basic requirement is to adequately resolve all significant features of the flow. The commonly accepted criteria of a mesh Reynolds number of the order of two is impractical for the present analysis[6] but also seems to be unnecessary.[16,17] For turbulent flow, the high-velocity gradients near the wall dictate an extremely fine mesh spacing to achieve adequate numerical resolution. The exponential stretching of the grid-spacing immediately adjacent to the wall combined with a coarser constant step-size in the outer region is used in the normal direction of the main flow.[4,16,17]

In the present analysis, the entire flowfield is divided into two overlapping computational domains. In the first domain, the development of a turbulent boundary layer over a flat plate is calculated. The interacting region is contained within the second computational domain, which overlaps the first region. The calculations are joined at $x = 0.8749$ ft from the leading edge. A 64×30 calculation mesh system is employed for both computational domains. The mesh point distribution in the normal coordinate includes 18 points in an exponentially varying inner region (Δy min $= 10^{-4}$ ft) and 12 points in the constant step-size outer region with Δy of 3.65×10^{-3} ft. However, for the interaction zone (the second computational domain), the grid-spacing in the streamwise direction is reduced from that of the first computational domain by a factor of three to give a Δx of 3.98×10^{-3} ft. Thus, the computational inviscid-viscous interaction zone has a physical dimension of about $20\delta \times 5\delta$.

The present calculation was performed on a CDC 6600 computer, for which nearly full use was made of the available memory core. Increasing the dimensions of the inviscid-viscous interaction zone is still possible by simply overlapping additional computational domains. A similar procedure also can be used to perform a partial truncation error analysis. However, one feels that the basic issue of numerical resolution should be a separate and systematic effort and is beyond the scope of the present study. The convergence criteria required to obtain the asymptotic steady-state solution was defined to be 0.1% change in consecutive skin friction coefficient calculations. The criterion is reached generally in approximately 2 hr for the cases investigated.

V. Discussion of Results

As indicated earlier, a primary objective of the study is to investigate the sensitivity of the previously developed[16,17] relaxation eddy viscosity model through comparison with experimental data for the shock impingement problem. Numerical solutions were obtained for the experimental conditions of Law.[26] General features of the computed flowfield were found to be very similar to that of the ramp configuration (see Fig. 1).

Numerical solutions are presented in three groups. First the entire flowfields of the compression ramp and shock boundary-layer interaction are presented. The second group of results are intended to reveal the numerical sensitivity of the relaxation length parameter, λ, by comparing the surface pressure and location of the separation and reattachment points with experimental measurements.[24] In the last group, detailed flowfield prediction in terms of the density contour are compared with the holographic interferograms.

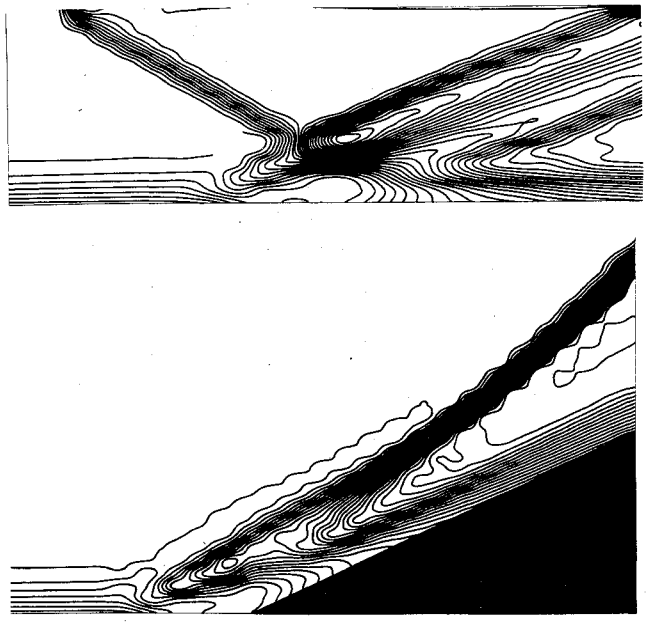

Fig. 1 Density contour graph of a compression ramp (25°) and shock-turbulent boundary-layer interaction (12.27°) for the same inviscid pressure rise.

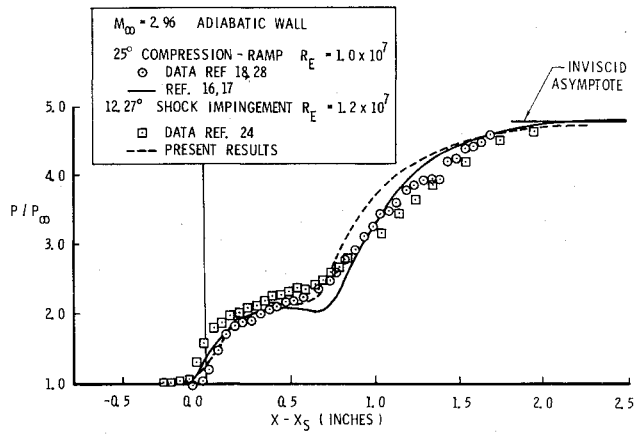

Fig. 2 Comparison of surface pressure distribution between a compression ramp (25°) and shock-turbulent boundary-layer interaction (12.27°).

In Fig. 1, two density contour graphs are presented together for the entire flowfield around a 25° compression ramp and a shock-boundary-layer interaction. The incident shock is induced by a 12.27° shock wave generator so that the inviscid pressure rise will be identical to the 25° ramp. The computed density contour graphs reproduce all the essential features of the supersonic interacting flowfield. For the compression ramp, a well-defined turbulent boundary layer is separated from the leading plate by the upstream pressure propagation. The separation shock penetrates well within the turbulent boundary layer. As the flow negotiates the corner and subsequently reattaches on the ramp, the reattachment shock wave system also appears. The separation shock and reattachment shock waves eventually coalesce downstream of the reattachment point. The shock boundary-layer interacting flowfield possesses nearly the identical general characteristics as the compression ramp. The expansion region imbedded between the separation shock and the reattachment shock waves of the shock boundary-layer interaction is substantially larger and more obvious than the ramp configuration. In this sense, Green[23] has correctly pointed out that the wave system produced by an incident oblique shock may be considered to be a variant of the compression ramp configuration.

An obvious shortcoming of the numerical solution is also revealed in the calculation of the incident shock. In "shock capturing," the thin incident oblique shock wave is smeared into a region with finite dimensions. In future work, it is recommended that this drawback be remedied by implementing a "shock fitting" scheme for the incident shock.[25-27] A "shock fitting" scheme in conjunction with the Navier-Stokes equations was successfully demonstrated recently by Tannehill, Holst, and Rakich[27] in their work on viscous blunt body flows with an impinging shock.

Although the computed incident shock yields the accurate shock-wave angle, the smearing of the shock creates a difficulty in the determination of an accurate coordinate reference point.[4,6,11,17,23] For that reason, the separation point is used as the coordinate origin consistently throughout the analysis.

The surface pressure distribution and regions of flow separation of a 25° ramp and shock-boundary-layer interaction generated by a 12.27° wedge are presented together with the experimental data[18,24] in Fig. 2. The compression ramp data and numerical solution were recorded for a Reynolds number of 10^7. The shock impingement data were collected for a Reynolds number of 1.2×10^7. The Mach number is identical for both cases. The overall agreement between the experiment and the computed pressure distribution is acceptable with the ramp configuration results, being slightly better than for shock impingement. The maximum deviation between the pressure data and the calculated value is about 15% based upon the downstream pressure. For both cases, the most serious discrepancy between data and computed results is in the region between the pressure plateau and the reattachment point.

In the next group of presentations (Figs. 3-6), the sensitivity of the relaxation length parameter, λ, in predicting the surface pressure distribution and location of separation and reattachment is demonstrated. The data were obtained for four different incident shock strengths by changing flow deflection angles of the shock generator. The deflection angles are given as 7.93° (Fig. 3), 8.90° (Fig. 4), 9.87° (Fig. 5), and 10.83° (Fig. 6). Two numerical computations with different relaxation length scales $\lambda = 10\delta_0$ and $\lambda = 20\delta_0$ were performed for all the cases considered.

The differences between the calculations of $\lambda = 10\delta_0$ and $\lambda = 20\delta_0$ are concentrated around the flow separation and the reattachment regions. Doubling the relaxation length parameter λ produces only a maximum change in pressure level and the size of the reverse flow region of approximately 20%. The calculations with $\lambda = 20\delta_0$ produces better agreement with Law's data than the numerical solutions with $\lambda = 10\delta_0$. Serious disparity appears only in the prediction of the pressure plateau and in the reattachment region (Figs. 3-6). Part of the discrepency is possibly caused by the approximation of Reynolds stress by the eddy viscosity coefficient, particularly in the separated region. Detailed experimental measurements of the Reynolds stress are needed in the reverse-flow region to resolve this issue.

The difference between the numerical results is exclusively produced by the different relaxation length scales. However, the possible source of the differences between the numerical results and experimental results cannot be easily identified. According to Green[23] and Law,[28] substantial variations exist between experimental measurements performed under supposedly similar conditions in different facilities.[23,28,29] This problem is particularly acute for shock wave-boundary-layer interaction investigations. Nevertheless, it is generally agreed that the discrepancies are primarily due to three-dimensional effects, but a specific evaluation has not been accomplished. It can be stated, however, that the numerical results are well within the experimental uncertainty of the measurements.

As in the investigation of compression ramps, one can follow the progression of increasing incident shock strength to

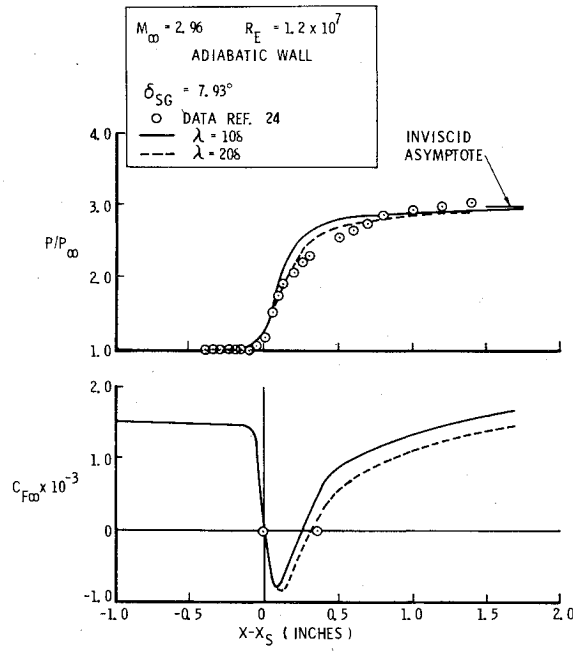

Fig. 3 Comparison of skin-friction coefficient and surface pressure distribution, $\delta_{sg} = 7.93°$.

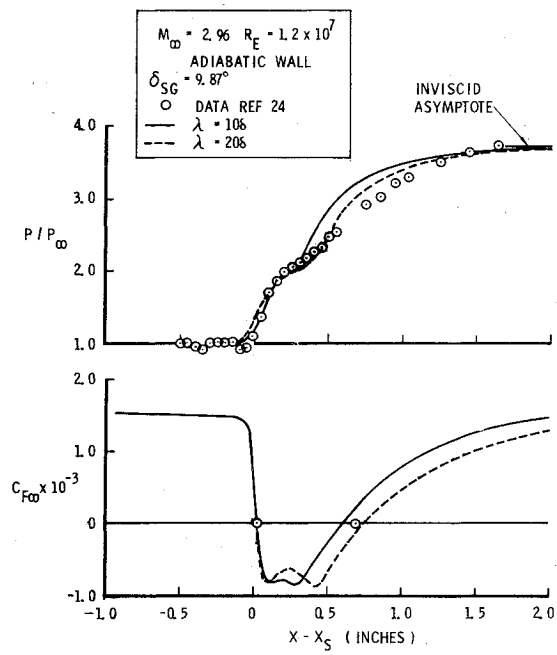

Fig. 5 Comparison of skin-friction coefficient and surface pressure distribution, $\delta_{sg} = 9.87°$.

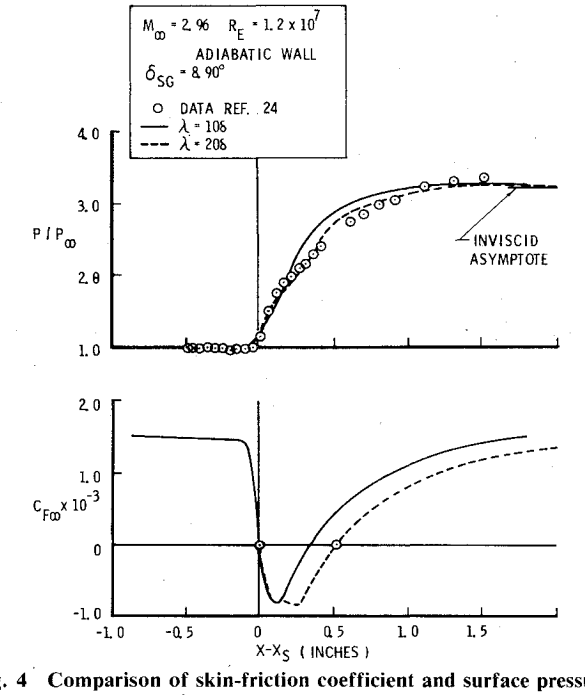

Fig. 4 Comparison of skin-friction coefficient and surface pressure distribution, $\delta_{sg} = 8.90°$.

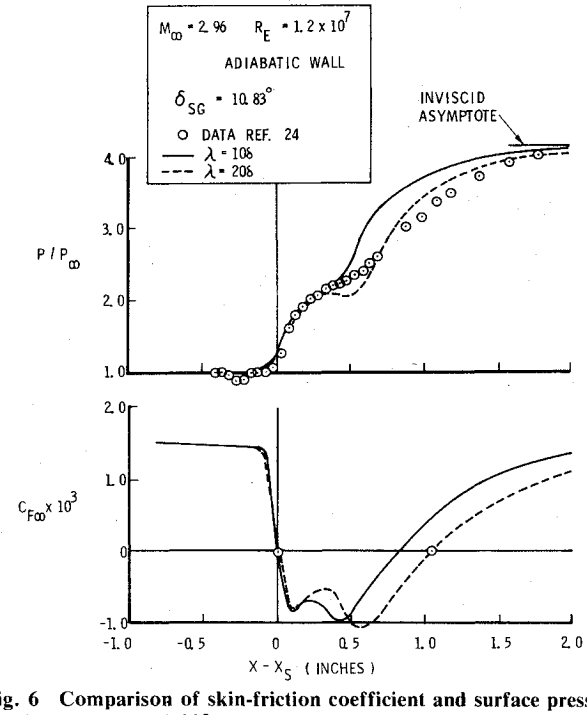

Fig. 6 Comparison of skin-friction coefficient and surface pressure distribution, $\delta_{sg} = 10.83°$.

observe the development of a pressure plateau and the "dual-minima" behavior in the skin friction coefficient distributions (Figs. 3-6). The overall agreements between data and the numerical prediction is considered to be acceptable for engineering applications. Baldwin and Rose also reached the identical conclusion in their calculation of shock-separated turbulent boundary layers.[30]

Comparisons are made between measured and calculated flowfield density distributions (see Figs. 7-10). The calculated density contours are compared with the experimental holographic interferograms, and the calculated density profiles at several selected streamwise locations are compared with measured profiles obtained from the interferograms. The holographic interferograms contain the three-dimensional effects that emanate from the corner region near the wind tunnel sidewalls. Upstream of the interaction region, these effects are minimal. However, in the interaction zone and downstream, the errors can be quite significant if three-dimensional effects are not accounted for. The detailed data reduction procedure for obtaining density profiles from the interferograms is discussed in Ref. 31. Although this procedure estimates the three-dimensional effects, actual measurements of density can be as much as 15 to 20% in error. However, spatial resolution is quite accurate, to within 0.005 in. The numerical solutions duplicate the essential features of the flowfield and in general are within the uncertainty envelope of the experimental data.

The density contour plots and interferograms are in general agreement. The computed density contours (Figs. 7-10) indicate clearly that the incident shock penetrates deeply into

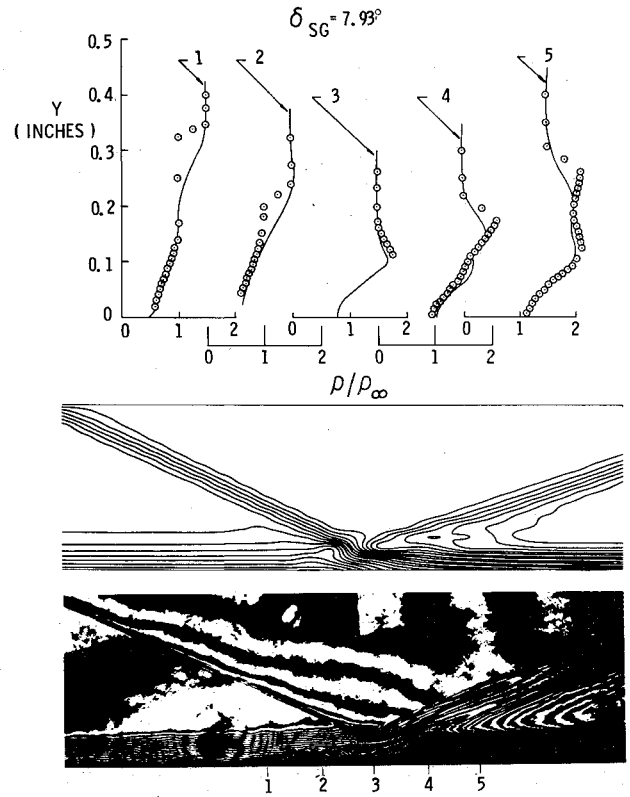

Fig. 7 Comparison of density contours holographic interferogram and density profiles, $\delta_{sg} = 7.93°$.

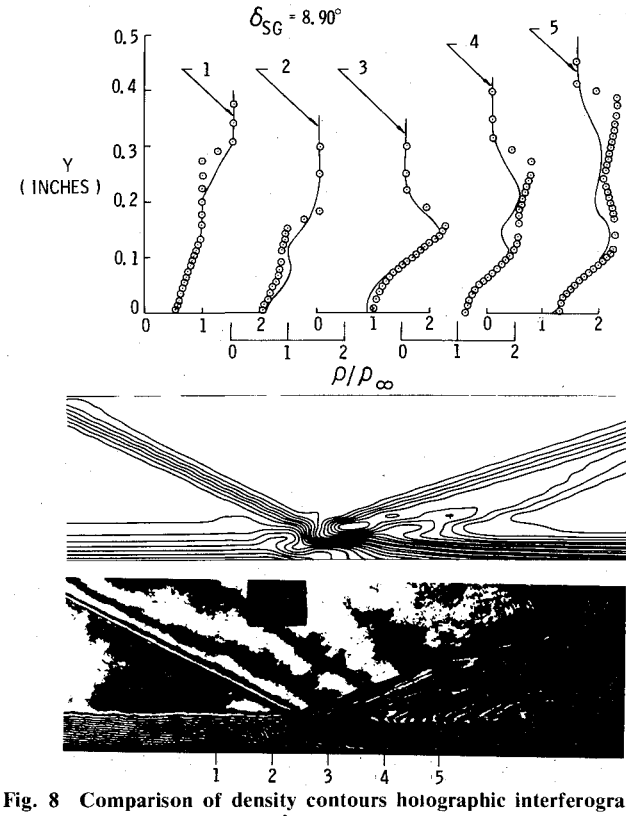

Fig. 8 Comparison of density contours holographic interferogram and density profiles, $\delta_{sg} = 8.90°$.

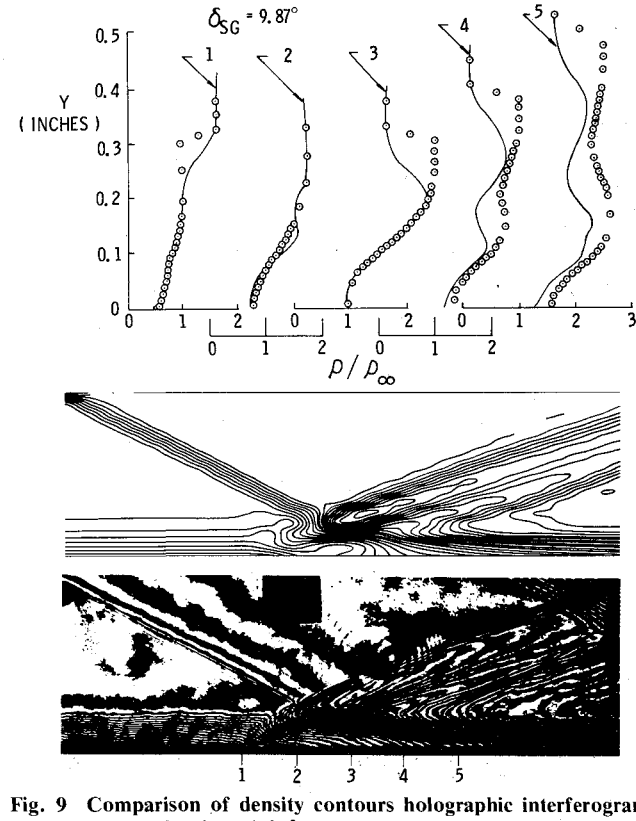

Fig. 9 Comparison of density contours holographic interferogram and density profiles, $\delta_{sg} = 9.87°$.

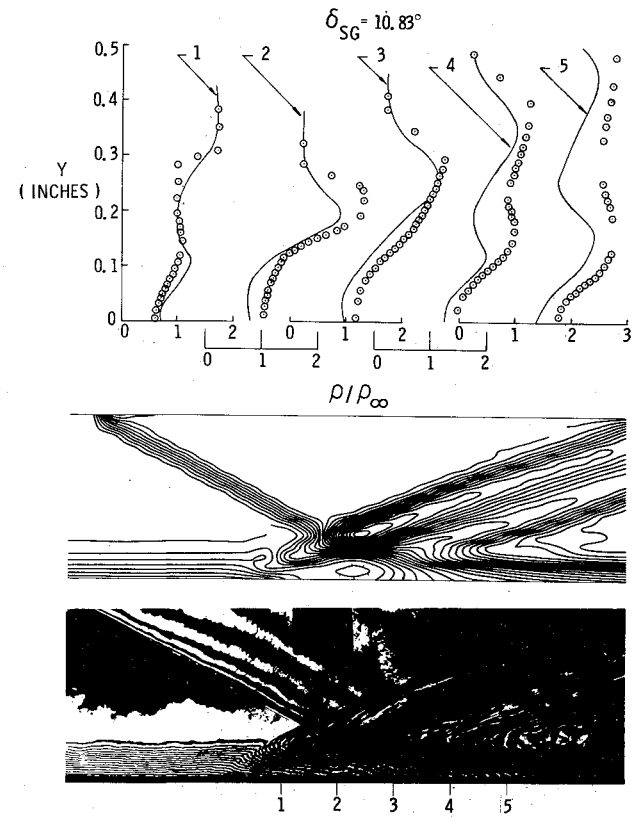

Fig. 10 Comparison of density contours holographic interferogram and density profiles, $\delta_{sg} = 10.83°$.

the turbulent boundary layer. The severe adverse pressure gradient causes boundary-layer separation. The separation not only induces an upstream pressure propagation but also triggers a family of compression wavelets, which coalesce to form the separation shock. An imbedded expansion region immediately follows to compensate for the over compression.

As the separated shear layer reattaches to the plate, the shear layer realigns with the plate and induces a second group of compression wavelets, which coalesce to form the reattachment shock. Far downstream of the shock impingement

point, the turbulent boundary layer re-emerges into a highly compressed region. The separation and reattachment shock eventually coalesce to form the classic reflected shock wave. The numerical results accurately predict the incident shock strength and overall pressure rise (see Figs. 3-6) for the inviscid pressure asymptotes). However, the contour plots and density profiles reveal considerable shock smearing produced by the present coarse grid size employed in the inviscid region. (In principle, an improvement in the definition of the incident shock wave is possible by adopting a "shock fitting" scheme).[27] For the impinging shock of relatively weak strength, a good agreement of density profiles between experiments and calculations is obtained. In summary, this present effort demonstrates the feasibility of computing the interaction of a shock wave with a turbulent boundary layer.

VI. Conclusion

After completing the compression ramp study[16,17] further verification of the relaxation turbulence model was deemed appropriate. Therefore, shock impingement on a turbulent boundary layer was studied. A comparison of the numerical solutions with experimental measurements by Law[24,28] was made. A parametric study of the relaxation length scale λ, showed the value of $20\delta_0$ to be superior to $10\delta_0$ as previously used for the study of compression ramps. Comparison of the pressure, skin friction distribution, and density contours with the experiment exhibited good engineering agreement. The shock boundary-layer interacting flowfield possesses nearly the identical characteristics to that of the compression ramp. This finding substantiates Green's assertion that the wave system produced by an incident oblique shock may be considered to a variant of the flow over a compression ramp.[23]

Improvements on the present analysis were identified and recommended for future work.

a) Due to the large step size of the grid, the incident shock was smeared which propagated an error downstream. A "shock fitting" scheme[25-27] is recommended to eliminate this deficiency.

b) An improvement of the turbulence model in the separated region is recommended in order to improve the agreement in the pressure plateau region.

References

[1] Dwoyer, D. L., "Supersonic and Hypersonic Two-Dimensional Laminar Flow Over a Compression Corner," *Proceedings AIAA Computational Fluid Dynamics Conference,* 1973, pp. 69-77.

[2] Werle, M. J. and Vatsa, V. N., "Numerical Solution of Interacting Supersonic Boundary Layer Flows Including Separation Effects," ARL TR 73-0162. Aerospace Research Laboratories, Wright-Patterson AFB, Ohio, Dec. 1973.

[3] Carter, J. E., "Solutions for Laminar Boundary Layers with Separation and Reattachment," AIAA Paper 74-583, Palo Alto, Calif., 1974.

[4] MacCormack, R. W., "Numerical Solutions of the Interaction of a Shcok Wave with a Laminar Boundary Layer," *Lecture Notes in Physics,* Vol. 8, Springer-Verlag, New York, 1971, pp. 151-163.

[5] Carter, J. E., "Numerical Solution of the Supersonic Laminar Flow Over a Two-Dimensional Compression Corner," *Lecture Notes in Physics,* Vol. 19, Springer-Verlag, New York, 1973, pp. 69-78.

[6] MacCormack, R. W. and Baldwin, B. S., "A Numerical Method for Solving the Navier-Stokes Equations With Application to Shock-Boundary Layer Interactions," AIAA Paper 75-1, Pasadena, Calif., 1975.

[7] Hung, C. M. and MacCormack, R. W., "Numerical Solutions of Supersonic and Hypersonic Laminar Flows Over a Two-Dimensional Compression Corner," AIAA Paper 75-2, Pasadena, Calif., 1975.

[8] Stewartson, K. and Williams, P. G., "Self-Induced Separation," *Proceedings of the Royal Society, Series A, Mathematical and Physical Sciences*, Vol. 213, 1969, pp. 181-206.

[9] Burggraf, O. R., "Asymptotic Theory of Separation and Reattachment of a Laminar Boundary Layer on a Compression Ramp," AGARD Conference on Flow Separation, Gottingen, Germany, AGARD-CPP-168, May 1975, pp. 10-1, 10-9.

[10] Jensen, R., Burggraf, O. R., and Rizzetta, D. P., "Asymptotic Solution for Supersonic Viscous Flow Past a Compression Corner," *Proceedings of 4th International Conference on Numerical Methods in Fluid Dynamics*, Boulder, Colorado, June 1974.

[11] Wilcox, D. C., "Numerical Study of Separated Turbulent Flows," AIAA Paper 74-584, Palo Alto, Calif., 1974.

[12] Saffman, P. G. and Wilcox, D. C., "Turbulence Model Predictions for Turbulent Boundary Layer," *AIAA Journal*, Vol. 12, April 1974, pp. 541-546.

[13] Baldwin, B. S. and MacCormack, R. W., "Numerical Solution of the Interaction of a Strong Shock Wave with a Hypersonic Turbulent Boundary Layer," AIAA Paper 74-558, Palo Alto, Calif., 1974.

[14] Cebeci, T., Smith, A. M. O., and Mosinskis, G., "Calculations of Compressible Adiabatic Turbulent Boundary Layer," *AIAA Journal*, Vol. 8, No. 11, Nov. 1970, pp. 1974-1982.

[15] Horstman, C. C., Kussoy, M. I., Coakley, T. J., Rubesin, M. N., and Marvin, J. G., "Shock-Wave Induced Turbulent Boundary-Layer Separation at Hypersonic Speeds," AIAA Paper 75-4, Pasadena, Calif., 1975.

[16] Shang, J. S. and Hankey, W. L., Jr., "Numerical Solution of the Navier-Stokes Equations for Supersonic Turbulent Flow Over a Compression Ramp," AIAA Paper 75-3, Pasadena, Calif., 1975.

[17] Shang, J. S. and Hankey, W. L., Jr., "Supersonic Turbulent Flows Utilizing the Navier-Stokes Equations," AGARD Conference on Flow Separation, Gottingen, Germany, AGARD-CPP-168, May 1975, pp. 23-31.

[18] Law, C. H., "Supersonic Turbulent Boundary-Layer Separation," *AIAA Journal*, Vol. 12, June 1974, pp. 794-797.

[19] Deissler, R. G., "Evolution of a Moderately Short Turbulent Boundary Layer in a Severe Pressure Gradient," *Journal of Fluid Mechanics*, Vol. 64, 1974, pp. 763-774.

[20] Narasimha, R. and Prabhu, A., "Equilibrium and Relaxation in Turbulent Wakes," *Journal of Fluid Mechanics*, Vol. 54, 1972, pp. 1-17.

[21] Bradshaw, P., "Effects of Streamline Curvature on Turbulent Flow," AGARD, Gottingen, Germany, AGARD-AG-169, Aug. 1973.

[22] Rose, W. E. and Johnson, D. A., "A Study of Shock-Wave Turbulent Boundary Layer Interaction Using Laser Velocimeter and Hot-Wire Anemometer Techniques," AIAA Paper 74-95, Washington, D. C., 1974.

[23] Green, J. E., "Interaction Between Shock Waves and Turbulent Boundary Layer," *Progress in Aerospace Sciences*, Vol. 11, Pergamon, New York, 1970, pp. 235-340.

[24] Law, C. H., "Supersonic Shock Wave–Turbulent Boundary Layer Interactions," AIAA Paper 75-832, Hartford, Conn., 1975.

[25] Kutler, P., Reinhardt, W. A., and Warming, R. F., "Multi-Shocked, Three-Dimensional Supersonic Flowfields with Real Gas Effects," *AIAA Journal*, Vol. 11, May 1973, pp. 657-664.

[26] Moretti, G., "Floating Shock Fitting Technique Imbedded Shocks in Unsteady Multi-Dimensional Flows," *Proceedings of the 1974 Heat Transfer and Fluid Mechanics Institute*, Stanford University Press, Stanford, Calif., 1974, p. 184.

[27] Tannehill, J. C., Holst, T. L., and Rakich, J. V., "Numerical Computation of Two-Dimensional Viscous Blunt Body Flows with an Impinging Shock," AIAA Paper 75-154, Pasadena, Calif., 1975.

[28] Law, C. H., "Two-Dimensional Compression Corner and Planar Shock Wave Interactions with a Supersonic, Turbulent Boundary Layer; ARL TR 75-0157, Aerospace Research Labs, Wright-Patterson AFB, Ohio, Feb. 1975.

[29] Reda, D. C. and Murphy, J. D., "Shock-Wave-Turbulent Boundary Layer Interactions in Rectangular Channels, Part II; The Influence of Sidewall Boundary Layers on Incipient Separation and Scale of the Interaction," AIAA Paper 73-234, Washington, D. C., 1973.

[30] Baldwin, D. S. and Rose, W. E., "Calculation of Shock-Separated Turbulent Boundary Layers," NASA SP-347, March 1975.

[31] Havener, A. G. and Radley, R. J., "Supersonic Wind Tunnel Investigations Using Pulsed Laser Holography," Aerospace Research Laboratories, Wright-Patterson AFB, Ohio, ARL 73-0148, Oct. 1973.